Oxygen permeation flux through 10Sc1YSZ-MnCo2O4 asymmetric membranes prepared by two-step sintering

Pirou, Stéven; Gurauskis, Jonas; Gil, Vanesa; Søgaard, Martin; Hendriksen, Peter Vang; Kaiser, Andreas; Ovtar, Simona; Kiebach, Wolff-Ragnar

Published in:
Fuel Processing Technology

Link to article, DOI:
10.1016/j.fuproc.2016.06.019

Publication date:
2016

Document Version
Peer reviewed version

Oxygen permeation flux through 10Sc1YSZ-$MnCo_2O_4$ asymmetric membranes prepared by two-step sintering

*Stéven Pirou *[a], Jonas Gurauskis[a], Vanesa Gil[a], Martin Søgaard [a1], Peter Vang Hendriksen[a], Andreas Kaiser[a], Simona Ovtar[a], Ragnar Kiebach[a].*

[a] Department of Energy Conversion and Storage, Technical University of Denmark, Risø campus, Frederiksborgvej 399, DK-4000 Roskilde, Denmark

[1] Current address: Meneta Advanced Shims Technology A/S, Kirkegyden 52, DK-5270 Odense N, Denmark.

* Corresponding author: Tel: +45 93511217. E-mail address: stepir@dtu.dk.

Abstract

Asymmetric membranes based on a dual phase composite consisting of $(Y_2O_3)_{0.01}(Sc_2O_3)_{0.10}(ZrO_2)_{0.89}$ (10Sc1YSZ) as ionic conductor and $MnCo_2O_4$ as electronic conductor were prepared and characterized with respect to sinterability, microstructure and oxygen transport properties. The composite membranes were prepared by tape casting, lamination and fired in a two-step sintering process. Microstructural analysis showed that a gastight thin membrane layer with the desired ratio of ionic/electronic conducting phases could be fabricated. Oxygen permeation fluxes across the 10Sc1YSZ/ $MnCo_2O_4$ (70/30 vol.%) composite membrane were measured from 750 to 940°C using air or pure oxygen as feed gases and N_2 or CO_2 as sweep gases. Fluxes up to 2.3 $ml_N\ min^{-1}cm^{-2}$ were obtained for the 7 micron thick membrane. A degradation test over 1730 hours showed an initial degradation of 21% during the first 1100 hours after which stable performance was achieved. The observed degradation is attributed to coarsening of the infiltrated catalyst.

Keywords

Two-step sintering, Oxygen membranes, Composite membranes, Asymmetric membranes, Oxygen flux, CO_2 stability.

1. Introduction

To reduce global warming and adverse climate changes it is important to reduce anthropogenic CO_2. One possible approach to such emission reduction is to capture and sequester CO_2 from large point sources, e.g. fossil fuel power plants. Among the available technologies for Carbon Capture and Sequestration (CCS), oxy-fuel combustion is a promising option. This approach uses oxygen instead of air in the combustion process. By eliminating nitrogen from the oxidant gas stream, it is possible to produce a CO_2-enriched flue gas (90-95% CO_2 in the dried flue gas) and the non circulated part of the CO_2 can be compressed and stored [1]. The main energy demand for oxy-fuel process results from the oxygen production, which is today produced from cryogenic air separation units (ASU), the only available technology for large-scale production. However, cryogenic air separation is a highly energy consuming and expensive process [2][3], especially if small and medium scale combustion processes are considered. This energy demand could potentially be significantly lowered using thermally integrated separation modules based on ceramic oxygen transport membranes (OTM) [4][5].

Typical oxygen transport membranes consist of a gastight mixed ionic and electronic conductor (MIEC), which allows oxygen diffusion through vacancies in the crystal lattice and simultaneous transport of electrons in the opposite direction. Membranes based on single phase MIEC materials can achieve high oxygen fluxes [6], but unfortunately most of flux wise promising membrane materials are not chemically stable under atmospheres containing CO_2, SO_2 and H_2O; conditions which are going to be encountered with membrane integration in power plants that are suitable for CCS. The materials having adequate chemical stability unfortunately typically do not provide sufficient oxygen transport. For example, compounds in the $Ba_{1-x}Sr_xCo_{1-y}Fe_yO_{3-\delta}$ (BSCF) and $La_{1-x}Sr_xCo_{1-y}Fe_yO_{3-\delta}$ (LSCF) series have attracted large interest due to their good electronic and ionic conductivity [7][8][9][10][11], however, their lack of chemical stability in the presence of CO_2 [12][13][14][15][16][17] (especially for the alkaline earth rich and cobalt rich compounds) clearly show the limitations of these compounds for oxy-fuel applications involving direct integration. Indeed, for materials containing La and alkaline earth metals the stability in

CO_2 and SO_2 is low because of the potential formation of La/alkaline carbonates and sulphates. Carbonate formation at the surface of membrane reduces the surface exchange rate and consequently reduces the oxide ion transport through the membrane. In contrast, ionic conductors like doped zirconia ($(ZrO_2)_{1-x}(Y_2O_3)_x$ (YSZ), $(ZrO_2)_{1-x}(Y_2O_3)_x(Sc_2O_3)_y$ (ScYSZ)) or doped ceria ($Ce_{1-x}Gd_xO_{2-\delta}$ (CGO), $Ce_{1-x}Sr_xO_{2-\delta}$ (CSO), $Ce_{1-x}Pr_xO_{2-\delta}$ (CPO)) have high chemical stability in CO_2 and at low oxygen partial pressure. Fluxes in membranes constructed from such materials is strongly limited by electronic conductivity [18] [19].

Dual phase systems, where the membrane consists of a composite of a stable ionic conductor and a stable electronic conductor, can therefore be an alternative to the single phase system to ensure high oxygen flux and chemical stability at the same time.

Early reported dual phase membranes were ceramic-metal (cermet) composites consisting of an oxygen ion-conducting oxide phase and an electron-conducting noble metal phase ($(ZrO_2)_{1-0.08}(Y_2O_3)_{0.08}$/Pt [20] and Bi_2O_3-Er_2O_3/Au [21]). The price of the membrane can strongly be decreased avoiding the noble metals by using only ceramic compounds (“cer/cer”). Such “cercer”, e.g. composite membranes $NiFe_2O_4$ - $Ce_{0.9}Gd_{0.1}O_{1.95}$ (NFO-CGO10) [17] and $Ce_{0.8}Gd_{0.2}O_{1.9}$ - $MnFe_2O_4$ (CGO-MFO) [22] have indeed been shown to be stable in CO_2.

The thermodynamic driving force for oxygen transport through a MIEC membrane is the oxygen chemical potential gradient across the membrane, dictated by the imposed oxygen activities on the two sides of the membrane. The flux through the membrane is for the case of fast surface exchange given by the Wagner Equation (1):

$$J_{O_2} = \frac{RT}{16F^2L}\int_{P''_{O_2}}^{P'_{O_2}} \frac{\sigma_e\sigma_i}{\sigma_e+\sigma_i}\,(pO_2)\; d\ln pO_2 \qquad (1)$$

where J_{O_2} is the oxygen permeation flux (mol m^{-2} s^{-1}), R is the gas constant, F is the Faraday constant, L is the membrane thickness, σ_e and σ_i are the electronic and the ionic conductivities, and P'_{O_2} and P''_{O_2} are the oxygen partial pressures at the high pressure side and low pressure side, respectively.

In order to obtain a high oxygen flux, the membrane should evidently (cf. Eq 1) be as thin as possible. Asymmetric membranes, which combine a relatively thick porous support (for mechanical stability) and a thin dense membrane layer, are a promising architecture to minimize the actual membrane thickness whilst ensuring mechanical robustness.

To manufacture dual phase asymmetric membranes, the following material related challenges must be overcome: (i) a heat treatment which allows a proper co-sintering of all layers must be established, (ii) the two materials must be chemically compatible ensuring no (or very limited) reaction between the two phases, and finally (iii) the thermal expansion coefficients (TECs) between the membrane materials and the support must be very close to ensure mechanical integrity of the component.

Yttria stabilized zirconia (YSZ) has been studied as the ionic conductor in composite OTMs due to its high ionic conductivity, its thermodynamic stability in oxidizing and reducing atmospheres and its good mechanical strength [18]. The highest ionic conductivity for $(ZrO_2)_{1-x}(Y_2O_3)_x$ electrolytes is observed for x=0.08 (8YSZ) and is around 0.03 S/cm at 850°C [23]. Further addition of Y_2O_3 will decrease the ionic conductivity due to enhanced association of the oxygen vacancies and dopant cations, which results in defect-complexes with low mobility [24]. Co-doping of scandium and yttrium in zirconia results in significant enhancement of the ionic conductivity as compared with 8YSZ. Artemov et al. reported that the ionic conductivity of $(Y_2O_3)_{0.01}(Sc_2O_3)_{0.10}(ZrO_2)_{0.89}$ (10Sc1YSZ) is higher than 0.12 S/cm at 850°C [25]. Therefore, 10Sc1YSZ was chosen here as the ionic conductor for the dual phase membrane.

Spinels containing manganese and cobalt are known to possess high electrical conductivity [26]. The electrical conductivity of $MnCo_2O_4$ is reported to be in the range of 60-100 S/cm at 800-900°C [27][28]. In addition, $MnCo_2O_4$ is much easier to sinter than many other spinel-type oxides, and has a thermal expansion coefficient (TEC) (9.7 ppm/K between room temperature and 1000°C) [27] which is close to the TEC of 8YSZ (10.88 ppm/K [29] from room temperature to 1000°C). These properties make it a promising candidate as the electronic conductor in a dual phase system with 10Sc1YSZ (10Sc1YSZ-$MnCo_2O_4$). Yi *et al.* reported that the $MnCo_2O_4$ spinel starts to decompose by formation of cobalt oxide above 1200 °C [30], which is close to the required sintering temperature for the densification of YSZ. Therefore, it is expected to be difficult to fully densify a composite of $MnCo_2O_4$ and Sc1YSZ in an asymmetric membrane by conventional sintering.

Originally proposed by Chen and Wang, two-step sintering profiles allow producing nanostructured materials with high density at modest temperature, due to different grain growth and densification kinetics [31]. Indeed, with well chosen two-step sintering profiles the densification can proceed without grain growth. The suppression of the final-stage grain growth is achieved by exploiting the difference in kinetics between grain-boundary diffusion and grain-boundary migration. A typical two-step sintering profile consists of a first step with a fast heating rate (15-25 °C/min) to a peak temperature (without or with very short holding time (3 minutes maximum)) and, on a second step, the immediate cooling down to an isothermal plateau at a lower temperature. In the case of a composite membrane such a profile could allow a higher densification to achieve the desired microstructure in the composite membrane layer (and the porous support) while avoiding undesirable phase decompositions.

In this work we present how two-step sintering can be utilized to prepare planar asymmetric membranes consisting of a 10Sc1YSZ/$MnCo_2O_4$ composite. The membranes were manufactured by tape-casting, lamination and subsequently sintered in a two-step firing. First a sintering study is presented involving the laminated membranes heat treated at three different sintering profiles. This

allowed manufacturing of fully dense membranes. Catalysts were applied at both surfaces and oxygen permeation measured under different atmospheres. Finally a durability test was conducted with CO_2 as sweep gas.

2. Experimental

2.1. Membrane preparation

As presented in Figure 1, the asymmetric membranes consist of a 200 micron thick porous support (3YSZ + 20 vol.% of Al_2O_3) and a thin dense composite membrane layer (10Sc1YSZ/$MnCo_2O_4$, 7 µm) surrounded by two porous layers (8YSZ, 10 µm) that can be impregnated with a suitable catalyst. All layers were manufactured separately by tape casting. The YSZ (3YSZ and 8YSZ), 10Sc1YSZ and $MnCo_2O_4$ powders were purchased from Tosoh (Japan), Daiichi Kigenso Kagaku Kogyo Co. Ldt (Japan), and Marion Technologies (France), respectively. 3YSZ and 8YSZ powders were calcined for 2 h at 1100°C and 900°C, respectively prior to further processing. All materials were ball milled in ethanol to obtain particles within submicronic range. Three slurries were prepared and cast: (i) a slurry for the porous support layer containing 33 wt.% of pore formers in relation to the total solid content (Graphite (d_{v50}=7 µm) and PMMA (d_{v50}=1.8 µm) supplied by Graphit Kropfmühl AG (Germany) and Esprix Technologies (USA), respectively) (ii) a slurry for the porous functional layers containing 33 wt.% of pore former (PMMA) and (iii) a slurry for the membrane layer free of pore former.

After drying, the green tapes were assembled by lamination at 135°C and 30 mm diameter disks were cut out using a stamping tool.

As is presented in Figure 2, a sintering study was performed with following process parameters: (i) conventional sintering at 1250°C for 6 h, (ii) conventional sintering at 1075°C for 6 h (iii) two-step sintering, including a peak temperature of 1250°C (3 min) and a dwell temperature of 1075°C (6 h) (iv) two-step sintering at peak (3 min)/dwell (6 h) temperatures of 1225/1090°C. Heating rates of 0.25 °C/min

for the de-bindering and 1 °C/min for the sintering regime were used in all cycles. A holding time of 4 h at 600°C was implemented in all sintering profiles to ensure complete removal of organic matter. A heating ramp of 25 °C/min was used for the peak of the two-step sintering profiles. A dwell period of six hours was employed in all four sintering cycles. Figure 2 focuses on the last 30 hours of the sintering cycles since they distinguish the four sintering cycles. Table 1 summarizes the complete sintering cycles used to optimize the microstructure of the 10Sc1YSZ-$MnCo_2O_4$ asymmetric membranes. The obtained samples were characterized and compared by: (i) SEM analysis (fracture cross-section) and (ii) EDS analysis (polished cross-section).

After sintering, $Gd_{0.2}Ce_{0.8}O_{2-\delta}$ (GDC) and $LaNi_{0.6}Co_{0.4}O_{3-\delta}$ (LNC) aqueous solutions with concentration of 2.5 and 1.25 M were prepared by dissolving the corresponding nitrate solid solutions in water. The aqueous solutions were supplemented with a wetting agent (Triton X-100) and a complexing agent (Urea), and were infiltrated in both the porous YSZ layers to serve as oxygen oxidation/reduction catalysts. The samples were placed under vacuum to remove air and enhance the penetration of the solution into the porous support and the functional layers. This ensures an even distribution of the catalyst pre-cursor throughout the complete porous layers. The infiltrated samples were heat treated at 350 °C after each infiltration. The infiltration process was repeated 3 times for each aqueous solution, to ensure deposition of sufficient amounts catalyst in the porous layers. The impregnation procedure has been successfully applied in previous studies [32][33][34].

2.2. Membrane characterization

Contact dilatometry was used to determine the shrinkage and sintering activity of the porous support and the thin membrane layer materials. Rods (2 cm x 0.5 cm x 0.5 cm) of 3YSZ + 20 vol.% Al_2O_3 + 30 vol.% graphite and 10ScYSZ/$MnCo_2O_4$ (70/30 vol.%) powder mixtures were prepared by uniaxial pressing. Dilatometry on the dense bars was carried out on a Netzsch 402 CD differential dilatometer.

The bar of the porous support material was pre-calcined at 1000°C in order to avoid the destruction of the sample by the holder pressure of the dilatometer. The heating rate was 1°C/min from 1000°C to 1400°C. The 10ScYSZ/$MnCo_2O_4$ (70/30 vol.%) bar, was heated at 0.5°C/min from room temperature to 600°C, then 1°C/min from 600°C to 1250°C. All tests were performed in air.

The microstructure of the asymmetric membranes, and in particular the integrity of the thin film 10Sc1YSZ/$MnCo_2O_4$ layer, was investigated on fractured and polished cross-sections by scanning electron microscopy (SEM) using a Hitachi TM3000 equipped with a Bruker energy dispersive X-ray spectroscopy (EDS) system and a FE-SEM Zeiss Supra 35 electron microscope.

2.3. Oxygen permeation tests

Oxygen permeation measurements were conducted in an oxygen membrane rig built at Risø DTU as described by Samson *et al.* [35]. It consists of two alumina tubes that contact the membrane from the top and from the bottom. The gases are introduced to the interior of the test house to vicinity of sample and onto both sides of the membrane via smaller diameter alumina tubes inserted within the large, outer alumina tubes. The membrane is placed in the middle of a height adjustable tube furnace. Tape cast sodium aluminosilicate (NAS, Na_2O: 17.8 mol%, Al_2O_3: 9.4 mol% and SiO_2: 72.8 mol% [36]) glass rings, with an inner diameter of 9 mm, and a glass transition temperature of 515°C [35] were used as sealing material between the alumina tubes and the membrane. The side walls of the samples were also coated with NAS paste to ensure that no oxygen enters from the sweep gas compartment to the membrane. To ensure a gas tight sealing, the membrane was heated in air up to 940°C and afterwards cooled to 750°C. A gas chromatograph was connected to the outlet of the permeate side to quantify oxygen leak into the permeate stream (oxygen that enters the permeate compartment via pinholes or insufficient sealing at the membrane periphery). From a quantification of the leak the uncertainty of the measured permeation flux is less than 5%, mainly originated from the uncertainty of the area of the

tested membrane. During the test, air or pure O_2 with a flow of 100 $ml_N\ min^{-1}$ was fed to the feed side, while various flows of N_2 or CO_2 varying from 20 $ml_N\ min^{-1}$ to 150 $ml_N\ min^{-1}$ were fed to the permeate side. The membrane was assembled with the porous support on the feed side. The inlet flow of each gas was controlled and monitored by a mass flow controller (Brooks), while the outlet flow was determined by a mass flow meter (Bronkhorst). In the experiments reported here the flow out was equal to the flow in within 3%. In-house built zirconia-based pO_2 sensors were used to determine the pO_2 of the inlet gas on the permeate side (before feeding to the membrane) and of the outlet gas (after passing over the membrane). Net oxygen permeation flux was deduced from the pO_2 difference between inlet and outlet, as given by:

$$J_{O_2} = \frac{pO_2''\,\dot{n}'' - pO_2'\,\dot{n}'}{A} \qquad (2)$$

where J_{O_2} is the oxygen permeation flux, pO_2' and pO_2'' are respectively the oxygen partial pressures of the inlet and outlet gases, $\dot{n}'$ and $\dot{n}''$ are molar flow rates of inlet and outlet gases, respectively, and A is the net area of the permeate side of the membrane. The Nernst equation (3) is used to calculate the oxygen partial pressure from the measured sensor voltage (V):

$$V = \frac{R\,T}{4\,F}\ln\frac{pO_2}{pO_{2,ref}} \qquad (3)$$

where V is the open circuit voltage of the oxygen sensor, T is the temperature of the oxygen sensor and $pO_{2,ref}$ is the oxygen partial pressure at the reference electrode which was maintained at 0.21 atm during the measurement.

3. Results and Discussion

3.1. The effect of the sintering profile on the microstructure of 10Sc1YSZ/$MnCo_2O_4$ composite membranes

Simple percolation theory, assuming 6 nearest neighboring grains would predict a minimum of 33.3 vol.% of an electron conductive phase to form a continuous matrix in a composite system with random distribution of the phases. However, best consistence between the calculated and measured conductivity has in several systems been reported to be achieved with a slightly higher number of nearest neighboring grains [37][38]. Percolation is thus expected to be achievable below the 33%. In order to achieve the highest effective total conductivity in the membrane, a volume ratio between the ionic conductor (10Sc1YSZ) and electronic conductor ($MnCo_2O_4$) of 70:30 vol.% was chosen, reflecting that the ionic conductivity σ_{ionic} (0.12 S/cm at 850°C) [25] is five hundred time lower than the electronic conductivity $\sigma_{electric}$ (60 S/cm at 800°C) [27] and hence that one should use as much of the ionic conductor as possible while still maintaning percolation in the electronically conducting phase.

A critical step in the manufacturing of multi-layered membrane structures containing different ceramic materials is the optimization of the co-sintering process. In co-sintering, a good match of the shrinkage and strain rate of the different layers needs to be achieved in order to avoid the development of excessive stresses during sintering which can lead to mechanical failures [39]. For OTM applications, the thin membrane layer needs to be fully dense, while the support has to be sufficiently porous (usually 25-40% of porosity, depending on support thickness and microstructure) to assure sufficient permeability for gas supply and distribution.

Conventional sintering at 1250°C for 6 h in air (CS1250) did not result in a suitable microstructure for OTM use. Figure 3 presents the SEM/EDS analysis of the polished cross-section of the asymmetric membrane after conventional sintering. As shown in Figure 3a, the thin membrane layer is around 5 µm thick and completely densified. Nevertheless, the elemental maps of manganese and cobalt display that both elements which should be concentrated in the dense membrane layer are evenly distributed through all other layers. The manganese and cobalt mobility is too high at the chosen firing conditions. For this reason, a two-step sintering method (see pink and blue curves in Figure 2 corresponding to

TSS1250/1075 and TSS1225/1090 in Table 1) was subsequently attempted in order to fully densify the 10Sc1YSZ/$MnCo_2O_4$ dual phase membrane while at the same time; (i) avoiding excessive Co and Mn diffusions and (ii) ensuring a sufficient mechanical strength of the YSZ/Al_2O_3 support structure.

To elucidate the ideal sintering temperatures and optimize the sintering profile, separate dilatometry measurements were performed on the support and the membrane layer materials. The results of the dilatometry measurements are shown in Figure 4. The temperatures where densification occurs most rapidly are approximately 1200°C and 1025°C for the support and the thin membrane layer, respectively. In order to optimize the sintering, these two temperatures were chosen as the targeted dwell temperatures in the two stage sintering profiles. A temperature point close to the maximum shrinkage domain of the porous support was defined as a peak temperature for the short term sintering step. Sintering the membrane structure to this peak temperature should increase the density of the thin membrane layer and should ensure a good mechanical strength of the support. A temperature point close to the maximum densification of the thin membrane layer was selected for the second step dwell period. Such a sintering profile allows the membrane to sinter at relatively low temperature, and avoid the loss of $MnCo_2O_4$ experienced during conventional 6 h sintering at 1250°C (CS1250).

Figure 5 presents the SEM images of a fracture cross-sections and the elemental maps of Mn, Co and Sc obtained by EDS of membranes sintered using the sintering profiles described in Table 1 (TSS1250/1075, TSS1225/1090 and CS1075). Both membranes sintered using the two-step sintering method have fully dense membrane layers (Figures 5a and 5e). Their porosities were evaluated to be less than 1 vol.% by using a phase distribution analysis software. In comparison, the membrane which was conventionally sintered at 1075°C (CS1075) has a high porosity of 18 vol.%. Based on EDS results, the ratio of 10Sc1YSZ to $MnCo_2O_4$ in the thin membrane layer is about 75:25 vol.% (grains size: $d_{50\text{-}ScYSZ}$=1.01 µm and $d_{50\text{-}MnCo2O4}$=0.46 µm) in the case that the sintering profile (i) was used (TSS1250/1075, Figure 5b, 5c, 5d), while the same ratio is about 70:30 vol.% (grains size: $d_{50\text{-}ScYSZ}$=0.97 µm and $d_{50\text{-}}$

$_{MnCo2O4}$=0.51 μm) when the sintering profiles TSS1225/1090 (Figures 5f, 5g, 5h) or CS1075 (Figures 5j, 5k, 5l) were applied. These SEM/EDS results clearly show that the two-step sintering profiles allow on the densification of the 10Sc1YSZ/$MnCo_2O_4$ membrane layer without the loss of $MnCo_2O_4$ observed for the CS1075 one step profile.

3.2. Oxygen flux measurements on asymmetric dual-phase 10Sc1YSZ/$MnCo_2O_4$ membranes

The performance of the 10Sc1YSZ/$MnCo_2O_4$ (70/30 vol.%) asymmetric membranes on the 3YSZ support obtained by two-step sintering (TSS1225/1090) was evaluated carrying out oxygen permeation measurements, as described in Section 2.3.

Figure 6 displays the oxygen permeation flux as a function of the ratio between the oxygen partial pressures of the feed and permeate sides ($\ln(pO'_2/pO''_2)$) using N_2 and CO_2 as sweep gases, and pure oxygen as a feed gas. The flux scales in direct proportion to the driving force across the membrane. The highest fluxes in O_2/N_2 and O_2/CO_2 were measured at 940°C and correspond to 2.28 $ml_N\ min^{-1}\ cm^{-2}$ and 1.91 $ml_N\ min^{-1}\ cm^{-2}$, respectively. When air was used instead of pure oxygen as a feed gas, the fluxes decrease to 1.41 $ml_N\ min^{-1}\ cm^{-2}$ and 0.81 $ml_N\ min^{-1}\ cm^{-2}$, in N_2 and CO_2 respectively. Table 2 lists the values of oxygen permeation in different atmosphere at different temperatures. At temperature above 900°C, the oxygen permeation flux measured using CO_2 as the sweep gas is lower than that measured in N_2 at equivalent driving force. Several other studies of OTMs present lower performances in CO_2 when compared to N_2/He sweep [40][41][42][43][44][45]. The phenomenon has been suggested to be a consequence of suppressed oxygen surface exchange rate due to the chemisorption of CO_2 on the surface possibly blocking some oxygen vacancies [42][45].

When the permeation flux is limited not only by bulk diffusion but also by surface-exchange kinetics, the oxygen-permeation flux can, in a simple approximate description, be characterized by a modified Wagner equation (4) [46]:

$$J_{O_2} = -\frac{1}{1+(\frac{2L_c}{L})}\frac{RT}{16\ {}^2L}\int_{P''O_2}^{P'O_2}\frac{\sigma_{el}\sigma_{ion}}{\sigma_{el}+\sigma_{ion}}\ (pO_2)d\ln pO_2 \qquad (4)$$

where L_c (= D_a/K_s) is the characteristic membrane thickness, D_a is the ambi-polar diffusion coefficient and K_s is the surface-exchange coefficient. When the membrane thickness (L) is much smaller than L_c, the oxygen permeation is mainly limited by the surface-exchange kinetics, while for L $\gg L_c$ the bulk diffusion is the main rate limiting factor. Since $\sigma_{el} \gg \sigma_{ion}$ for 10Sc1YSZ/$MnCo_2O_4$ (70/30 vol.%) [25][27], the mixed conductivity term in the integrand in Eq. (5) becomes:

$$J_{O_2} = -\frac{1}{1+(\frac{2L_c}{L})}\frac{RT}{16F^2L}\int_{P''O_2}^{P'O_2}\sigma_{ion}\ (pO_2)d\ln pO_2 \qquad (5)$$

An approximate characteristic membrane thickness (L_c) was calculated from the O_2/N_2 experiments in comparing measured fluxes with the ones calculated from Equation 5 using known conductivity values for the zirconia treating L_c as a fitting parameter. For the calculations, we considered that: $\sigma_{ion,10Sc1YSZ} \gg \sigma_{ion,MnCo_2O_4}$, and approximated that $\sigma_{ion} = x * \sigma_{ion,10Sc1YSZ}$, where x is the volume percentage of 10Sc1YSZ in the composite membrane. The ionic conductivities of 10Sc1YSZ from 750 to 940 °C were taken from the study by Irvine *et al.* [47]. The driving force ln(pO_2'/pO_2") was fixed at 5 for the calculations.

Figure 7 presents the thus obtained L_c values as a function of the temperature and a comparison with the actual membrane thickness (L). For the complete investigated temperature range L_c is much larger than L (10 to 20 times) which strongly indicates that surface-exchange kinetics is a main rate limiting factor for the oxygen permeation. In case of gas concentration polarization on the permeate

side, the driving force will be overestimated which will result by a larger value of L_c. Calculations were performed at 950°C by using a lower driving force than assumed in order to show that even with gas concentration polarization effect L_c is significantly larger than L. Nevertheless, it is important to mention that in principal the ionic and electronic conductivities of the two phases in the membrane could deviate from the known materials values. For example, a modification of the microstructure, such as agglomeration of the phases could limit the percolation and therefore affect the conductivities. Also the ionic conductivity in the zirconia could in principle be reduced relative to that of the pure material due to interdiffusion of Mn, Co from the spinel. Moreover, the performed calculations do not consider a potential support limitation. A model developed by Niehoff et al. [48] introducing a surface correction factor for the calculation of L_c could be used to get more accurate results.

In order to investigate the chemical and thermal long-term stability of the dual phase membrane, the oxygen flux was measured for a continuous period of 1730 h with CO_2 as sweep gas and air as feed gas at 850°C. Figure 8 presents the evolution of the oxygen flux through the membrane as a function of the time (black line). The blue line represents the first derivative of the oxygen flux as a function of the time. For the first 1100 hours the flux decreases while after it stays constant for the last 600 hours of the experiment. Figure 9 shows SEM images of the very fine GDC and LNC particles infiltrated onto the functional membrane layer as oxygen oxidation/reduction catalysts. Before the oxygen permeation test, individual GDC/LNC particles are in the range of 20-50 nm (Figure 9a), while after 1730 h of testing in CO_2, they are in the range of 120-200 nm (Figure 9b). The particles thus clearly grow during the membrane operation. This coarsening causes a decrease in the surface area of the oxygen oxidation/reduction catalysts, therefore leading to surface exchange limitations. It is most likely the reason for the declining flux over the first 1100 hours.

4. Conclusions

Dual phase asymmetric 10Sc1YSZ/$MnCo_2O_4$ membranes were successfully prepared by tape casting, lamination and a two-step sintering process. The microstructure of the asymmetric membranes developed with different sintering cycles was studied and showed the advantages of the two-step sintering method to obtain a gastight membrane layer with the desired ratio of the ionic/electronic conductor. Such microstructures could not be obtained by conventional sintering. The oxygen permeation flux through a 7 μm 10Sc1YSZ/$MnCo_2O_4$ (70/30 vol.%) asymmetric membrane was studied from 750 to 940 °C under several atmospheres (air/pure oxygen as feed gases and N_2/CO_2 as sweep gases). An oxygen flux of 2.23 $ml_N\ min^{-1}cm^{-2}$ can be achieved at 940°C in O_2/N_2 atmospheres. A chemical and thermal stability test under CO_2 (as sweep gas) was performed over 1730 h and showed initial degradation during 1100 h, after which stable performance was observed during the remaining 630 h of test. The observed degradation is attributed to coarsening of the infiltrated catalyst phase. The 10Sc1YSZ/$MnCo_2O_4$ (70/30 vol.%) asymmetric membrane itself seems stable in CO_2 atmosphere and is thus a good candidate for use in industrial applications where the contact with CO_2 is required, for example for the use in oxy-coal fired power plants for Carbon Capture and Sequestration (CCS). Further improvement of the surface catalyst layers is needed to reach the full potential of these membranes.

Acknowledgments

The financial support from EU through the “Graded Membranes for Energy Efficient New Generation Carbon Capture Process (GREEN-CC)” project (Grant agreement no. 608524) is gratefully acknowledged. Karen Brodersen and Søren Preben Vagn Foghmoes are acknowledged by the authors for helping with tape-casting, and Henrik Paulsen for assisting in the preparation of the samples for SEM/EDS analysis.

References

[1] H. Stadler, F. Beggel, M. Habermehl, B. Persigehl, R. Kneer, M. Modigell, et al., Oxyfuel coal combustion by efficient integration of oxygen transport membranes, Int. J. Greenh. Gas Control. 5 (2011) 7–15. doi:10.1016/j.ijggc.2010.03.004.

[2] S.M. Hashim, A.R. Mohamed, S. Bhatia, Current status of ceramic-based membranes for oxygen separation from air, Adv. Colloid Interface Sci. 160 (2010) 88–100. doi:10.1016/j.cis.2010.07.007.

[3] S. Smart, C.X.C. Lin, L. Ding, K. Thambimuthu, J.C. Diniz da Costa, Ceramic membranes for gas processing in coal gasification, Energy Environ. Sci. 3 (2010) 268–278. doi:10.1039/b924327e.

[4] M. Czyperek, P. Zapp, H.J.M. Bouwmeester, M. Modigell, K. Ebert, I. Voigt, et al., Gas separation membranes for zero-emission fossil power plants: MEM-BRAIN, J. Memb. Sci. 359 (2010) 149–159. doi:10.1016/j.memsci.2010.04.012.

[5] S.S. Hashim, A.R. Mohamed, S. Bhatia, Oxygen separation from air using ceramic-based membrane technology for sustainable fuel production and power generation, Renew. Sustain. Energy Rev. 15 (2011) 1284–1293. doi:10.1016/j.rser.2010.10.002.

[6] J. Gurauskis, Ø. F. Lohne, D. S. Lagergren, E. T. Wefring, K. Wiik, Oxygen permeation in symmetric and asymmetric $La_{0.2}Sr_{0.8}Fe_{0.8}Ta_{0.2}O_{3-\delta}$ membranes, J. Eur. Ceram. Soc. Submitted. In progress.

[7] S. Baumann, J.M. Serra, M.P. Lobera, S. Escolástico, F. Schulze-Küppers, W. a. Meulenberg, Ultrahigh oxygen permeation flux through supported $Ba_{0.5}Sr_{0.5}Co_{0.8}Fe_{0.2}O_{3-\delta}$ membranes, J. Memb. Sci. 377 (2011) 198–205. doi:10.1016/j.memsci.2011.04.050.

[8] E. Perry Murray, M.J. Sever, S.A. Barnett, Electrochemical performance of $(La,Sr)(Co,Fe)O_3$-$(Ce,Gd)O_3$ composite cathodes, Solid State Ionics. 148 (2002) 27–34. doi:10.1016/S0167-2738(02)00102-9.

[9] A. Esquirol, J. Kilner, N. Brandon, Oxygen transport in $La_{0.6}Sr_{0.4}Co_{0.2}Fe_{0.8}O_{3-\delta}/Ce_{0.8}Ge_{0.2}O_{2-x}$ composite cathode for IT-SOFCs, Solid State Ionics. 175 (2004) 63–67. doi:10.1016/j.ssi.2004.09.013.

[10] P. Haworth, S. Smart, J. Glasscock, J.C. Diniz da Costa, High performance yttrium-doped BSCF hollow fibre membranes, Sep. Purif. Technol. 94 (2012) 16–22. doi:10.1016/j.seppur.2012.04.005.

[11] J. Sunarso, S. Baumann, J.M. Serra, W. a. Meulenberg, S. Liu, Y.S. Lin, et al., Mixed ionic-electronic conducting (MIEC) ceramic-based membranes for oxygen separation, J. Memb. Sci. 320 (2008) 13–41. doi:10.1016/j.memsci.2008.03.074.

[12] E. Bucher, A. Egger, G.B. Caraman, W. Sitte, Stability of the SOFC Cathode Material $(Ba,Sr)(Co,Fe)O_{3-\delta}$ in CO_2-Containing Atmospheres, J. Electrochem. Soc. 155 (2008) B1218. doi:10.1149/1.2981024.

[13] H. Luo, H. Jiang, K. Efimov, J. Caro, H. Wang, Influence of the preparation methods on the microstructure and oxygen permeability of a CO_2-stable dual phase membrane, AIChE J. 57 (2011) 2738–2745. doi:10.1002/aic.12488.

[14] M. Pilar Lobera, S. Escolastico, J. Garcia-Fayos, J.M. Serra, Ethylene Production by ODHE in Catalytically Modified $Ba_{0.5}Sr_{0.5}Co_{0.8}Fe_{0.2}O_{3-\delta}$ Membrane Reactors, ChemSusChem. 5 (2012) 1587–1596. doi:10.1002/cssc.201100747.

[15] S.J. Benson, D. Waller, J.A. Kilner, Degradation of $La_{0.6}Sr_{0.4}Fe_{0.8}Co_{0.2}O_{3-\delta}$ in Carbon Dioxide and Water Atmospheres, J. Electrochem. Soc. 146 (1999) 1305–1309.

[16] M. Schulz, R. Kriegel, A. Kämpfer, Assessment of CO_2 stability and oxygen flux of oxygen permeable membranes, J. Memb. Sci. 378 (2011) 10–17. doi:10.1016/j.memsci.2011.02.037.

[17] H. Luo, K. Efimov, H. Jiang, A. Feldhoff, H. Wang, J. Caro, CO_2-stable and cobalt-free dual-phase membrane for oxygen separation, Angew. Chemie - Int. Ed. 50 (2011) 759–763. doi:10.1002/anie.201003723.

[18] M.M. Hiroaki Yanagida, Kunihiko Koumoto, Kunihito Komoto, The Chemistry of Ceramics, 1996.

[19] T. Kawada, J. Suzuki, M. Sase, a. Kaimai, K. Yashiro, Y. Nigara, et al., Determination of Oxygen Vacancy Concentration in a Thin Film of $La_{0.6}Sr_{0.4}CoO_{3-\delta}$ by an Electrochemical Method, J. Electrochem. Soc. 149 (2002) E252. doi:10.1149/1.1479728.

[20] T.J. Mazanec, T.L. Cable, J.G. Frye, Electrocatalytic Cells for Chemical-Reaction, Solid State Ionics. 53 (1992) 111–118. doi:10.1016/0167-2738(92)90372-V.

[21] C.S. Chen, a J. Burggraaf, Stabilized bismuth oxide ± noble metal mixed conducting composites as high temperature oxygen separation membranes, J. Appl. Electrochem. 29 (1999) 355–360.

[22] H. Takamura, K. Okumura, Y. Koshino, A. Kamegawa, M. Okada, Oxygen permeation properties of ceria-ferrite-based composites, in: J. Electroceramics, 2004: pp. 613–618. doi:10.1007/s10832-004-5167-y.

[23] X.J. Chen, K.A. Khor, S.H. Chan, L.G. Yu, Influence of microstructure on the ionic conductivity of yttria-stabilized zirconia electrolyte, Mater. Sci. Eng. A. 335 (2002) 246–252. doi:10.1016/S0921-5093(01)01935-9.

[24] V. V. Kharton, E.N. Naumovich, A. a. Vecher, Research on the electrochemistry of oxygen ion conductors in the former Soviet Union. I. ZrO_2-based ceramic materials, J. Solid State Electrochem. 3 (1999) 61–81. doi:10.1007/s100080050131.

[25] V.G. Artemov, I.E. Kuritsyna, S.P. Lebedev, G. a Komandin, P.O. Kapralov, I.E. Spektor, et al., Analysis of electric properties of ZrO_2-Y_2O_3 single crystals using teraherz IR and impedance spectroscopy techniques, Russ. J. Electrochem. 50 (2014) 690–693. doi:10.1134/S1023193514070039.

[26] E. Rios, J.-L. Gautier, G. Poillerat, P. Chartier, Mixed valency spinel oxides of transition metals and electrocatalysis: case of the $Mn_xCo_{3-x}O_4$ system, Electrochim. Acta. 44 (1998) 1491–1497. doi:10.1016/S0013-4686(98)00272-2.

[27] A. Petric, H. Ling, Electrical conductivity and thermal expansion of spinels at elevated temperatures, J. Am. Ceram. Soc. 90 (2007) 1515–1520. doi:10.1111/j.1551-2916.2007.01522.x.

[28] M.Y. Yoon, E.J. Lee, R.H. Song, H.J. Hwang, Preparation and properties of a $MnCo_2O_4$ for ceramic interconnect of solid oxide fuel cell via glycine nitrate process, Met. Mater. Int. 17 (2011) 1039–1043. doi:10.1007/s12540-011-6025-5.

[29] H.L. Frandsen, T. Ramos, A. Faes, M. Pihlatie, K. Brodersen, Optimization of the strength of SOFC anode supports, J. Eur. Ceram. Soc. 32 (2012) 1041–1052. doi:10.1016/j.jeurceramsoc.2011.11.015.

[30] E.J. Yi, M.Y. Yoon, J.W. Moon, H.J. Hwang, Fabrication of a $MnCo_2O_4$/gadolinia-doped Ceria (GDC) dual-phase composite membrane for oxygen separation, J. Korean Ceram. Soc. 47 (2010) 199–204. doi:10.4191/KCERS.2010.47.2.199.

[31] I. Chen, X. Wang, Sintering dense nanocrystalline ceramics without final-stage grain growth, Nature. 404 (2000) 168–71. doi:10.1038/35004548.

[32] R. Kiebach, C. Knöfel, F. Bozza, T. Klemensø, C. Chatzichristodoulou, Infiltration of ionic-, electronic- and mixed-conducting nano particles into $La_{0.75}Sr_{0.25}MnO_3$–$Y_{0.16}Zr_{0.84}O_2$ cathodes – A comparative study of performance enhancement and stability at different temperatures, J. Power Sources. 228 (2013) 170–177. doi:10.1016/j.jpowsour.2012.11.070.

[33] T. Klemensø, C. Chatzichristodoulou, J. Nielsen, F. Bozza, K. Thydén, R. Kiebach, et al., Characterization of impregnated GDC nano structures and their functionality in LSM based cathodes, Solid State Ionics. 224 (2012) 21–31. doi:10.1016/j.ssi.2012.07.011.

[34] V. Gil; K. Kammer Hansen, High performance infiltrated backbones for cathode-supported SOFC's, ECS Trans. 64 (2014) 41–51. doi:10.1149/06402.0041ecst.

[35] A.J. Samson, M. Søgaard, P. Vang Hendriksen, $(Ce,Gd)O_{2-\delta}$-based dual phase membranes for oxygen separation, J. Memb. Sci. 470 (2014) 178–188. doi:10.1016/j.memsci.2014.07.028.

[36] K.A. Nielsen, M. Solvang, S.B.L. Nielsen, A.R. Dinesen, D. Beeaff, P.H. Larsen, Glass composite seals for SOFC application, J. Eur. Ceram. Soc. 27 (2007) 1817–1822. doi:10.1016/j.jeurceramsoc.2006.05.046.

[37] S.K. Bhattacharya, A.C.D. Chaklader, Review on Metal-Filled Plastics. Part1. Electrical Conductivity, Polym. Plast. Technol. Eng. 19 (1982) 21–51. doi:10.1080/03602558208067726.

[38] Wu Z. Modelling of ambipolar transport properties of composite mixed ionic-electronic conductors. Solid State Ionics 1996;93:65–84. doi:10.1016/S0167-2738(96)00521-8.

[39] G. Pećanac, S. Foghmoes, M. Lipińska-Chwałek, S. Baumann, T. Beck, J. Malzbender, Strength degradation and failure limits of dense and porous ceramic membrane materials, J. Eur. Ceram. Soc. 33 (2013) 2689–2698. doi:10.1016/j.jeurceramsoc.2013.04.018.

[40] W. Li, T. Tian, F. Shi, Y. Wang, C. Chen, for Oxygen Separation, Ind. Eng. Chem. Res. 48 (2009) 5789–5793. doi:10.1016/j.memsci.2012.03.026.

[41] K. Zhang, L. Liu, Z. Shao, R. Xu, J. Diniz da Costa, S. Wang, et al., Robust ion-transporting ceramic membrane with an internal short circuit for oxygen production, J. Mater. Chem. A. 1 (2013) 9150–9156. doi:10.1039/c3ta11427a.

[42] X. Tan, N. Liu, B. Meng, J. Sunarso, K. Zhang, S. Liu, Oxygen permeation behavior of $La_{0.6}Sr_{0.4}Co_{0.8}Fe_{0.2}O_3$ hollow fibre membranes with highly concentrated CO_2 exposure, J. Memb. Sci. 389 (2012) 216–222. doi:10.1016/j.memsci.2011.10.032.

[43] V. Esposito, M. Søgaard, P.V. Hendriksen, Chemical stability of $La_{0.6}Sr_{0.4}CoO_{3-\delta}$ in oxygen permeation applications under exposure to N_2 and CO_2, Solid State Ionics. 227 (2012) 46–56. doi:10.1016/j.ssi.2012.08.015.

[44] H. Luo, H. Jiang, K. Efimov, F. Liang, H. Wang, J. Caro, CO_2-Tolerant Oxygen-Permeable Fe_2O_3-$Ce_{0.9}Gd_{0.1}O_{2-\delta}$ Dual Phase Membranes, Ind. Eng. Chem. Res. 50 (2011) 13508–13517. doi:10.1021/ie200517t.

[45] J.M. Serra, J. Garcia-Fayos, S. Baumann, F. Schulze-Küppers, W. a. Meulenberg, Oxygen permeation through tape-cast asymmetric all-$La_{0.6}Sr_{0.4}Co_{0.2}Fe_{0.8}O_{3-\delta}$ membranes, J. Memb. Sci. 447 (2013) 297–305. doi:10.1016/j.memsci.2013.07.030.

[46] H.J.B. P. J. Gellings, The CRC Handbook of Solid State Electrochemistry, 1997.

[47] J.T.S. Irvine, J.W.L. Dobson, T. Politova, S.G. Martin, A. Shenouda, Co-doping of scandia-zirconia electrolytes for SOFCs., Faraday Discuss. 134 (2007) 41–49; discussion 103–118, 415–419. doi:10.1039/b604441g.

[48] P. Niehoff, S. Baumann, F. Schulze-Küppers, R.S. Bradley, I. Shapiro, W.A. Meulenberg, et al., Oxygen transport through supported $Ba_{0.5}Sr_{0.5}Co_{0.8}Fe_{0.2}O_{3-\delta}$ membranes, Sep. Purif. Technol. 121 (2014) 60–67. doi:10.1016/j.seppur.2013.07.002.

Figure captions:

Figure 1: Schematic structure of the 10Sc1YSZ/$MnCo_2O_4$ asymmetric membrane developed in this study, consisting of 4 layers from bottom to top: a porous 3 YSZ support layer, a porous 8YSZ layer to be impregnated with a catalyst, the 10Sc1YSZ/$MnCo_2O_4$ membrane layer and a second porous 8 YSZ for catalyst impregnation.

Figure 2: Four different sintering cycles used to optimize the microstructure of the 10Sc1YSZ-$MnCo_2O_4$ asymmetric membranes: (i) conventional sintering at 1250°C, (ii) conventional sintering at 1075°C, (iii) two-step

sintering at 1250°C/1075°C and (iv) two-step sintering at 1225°C/1090°C.The first 45 hours of the cycles are not shown since they are similar for the four different sintering cycles.

Figure 3: Polished cross-section of an asymmetric membrane after a conventional sintering at 1250C/6 h (CS1250) (a) SEM picture (b, c, d) EDS maps of Co, Mn and Sc elements.

Figure 4: Dilatometry curves, showing the shrinkage rate as function of sintering temperature for the porous support (a) and the thin membrane layer (b). Heating rate: 1°C/min.

Figure 5: SEM images and EDS maps (Mn, Co and Sc elements) of polished cross-sections of 10ScYSZ/MnCo2O4 asymmetric membranes TSS1250/1075 (a, b, c, d) TSS1225/1090 (e, f, g, h) and CS1075 (i, j, k, l).

Figure 6: Oxygen permeation flux of 10Sc1YSZ/$MnCo_2O_4$ (70/30 vol.%) membrane as a function of the natural logarithm ratio between the oxygen partial pressure of the feed and the permeate side using N_2 and CO_2 as a sweep gases and pure oxygen as a feed gas. The lines are a linear fit to the results.

Figure 7: The characteristic membrane thicknesses (L_c) as a function of temperature, for oxygen permeation fluxes obtained in O_2/N_2 with ln (pO_2'/pO_2'') = 5 (black) and 4 (blue).

Figure 8: Oxygen permeation flux through 10Sc1YSZ/$MnCo_2O_4$ (70/30 vol.%) composite membranes as a function of the time at 850°C, with constant flow of air as a feed gas and 112 $ml_N\ min^{-1}$ of CO_2 as a sweep gas.

Figure 9: SEM pictures of the GDC and LNC particles present onto the functional membrane layers prior to (a) and after (b) 1730 h of test in CO_2.

Table captions:

Table 1: Overview table of the four different sintering cycles used to optimize the microstructure of the 10Sc1YSZ-$MnCo_2O_4$ asymmetric membranes.

Table 2: Oxygen permeation fluxes ($ml_N\ cm^{-2}\ min^{-1}$) and driving force values through 10Sc1YSZ/$MnCo_2O_4$ (70/30 vol.%) asymmetric membrane as a function of the temperature and the used atmosphere.

Figure 1:

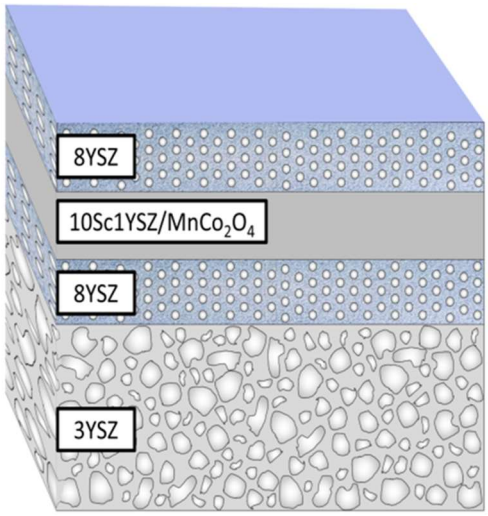

Figure 2:

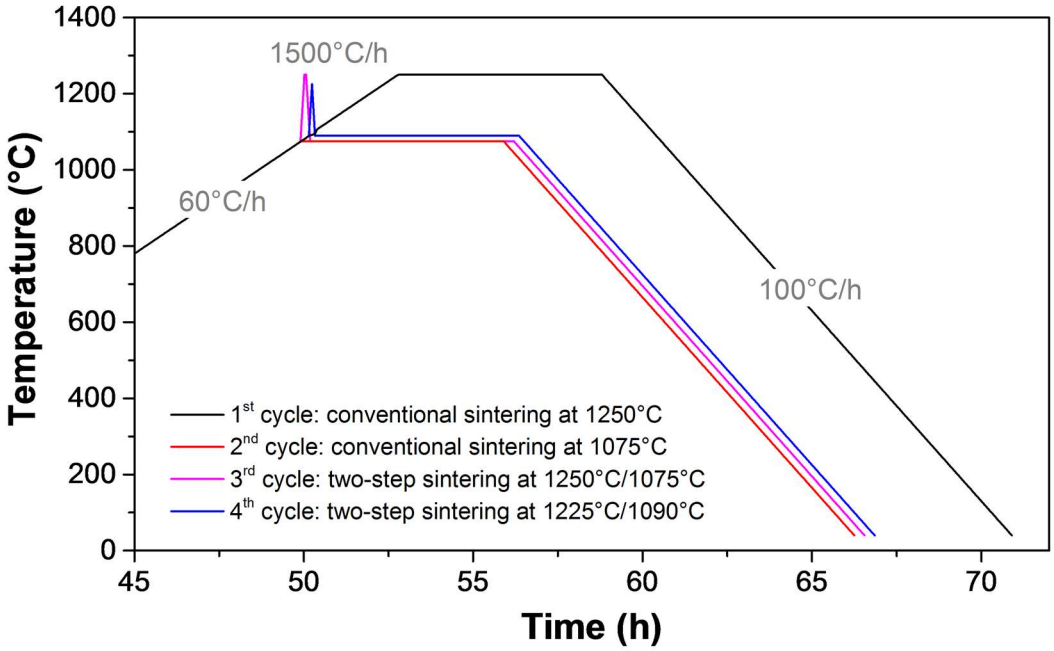
1400
1200
1000
800
600
400
200
0
Temperature (°C)
45
50
55
60
65
70
Time (h)
1500°C/h
60°C/h
100°C/h
1st cycle: conventional sintering at 1250°C
2nd cycle: conventional sintering at 1075°C
3rd cycle: two-step sintering at 1250°C/1075°C
4th cycle: two-step sintering at 1225°C/1090°C

Figure 3:

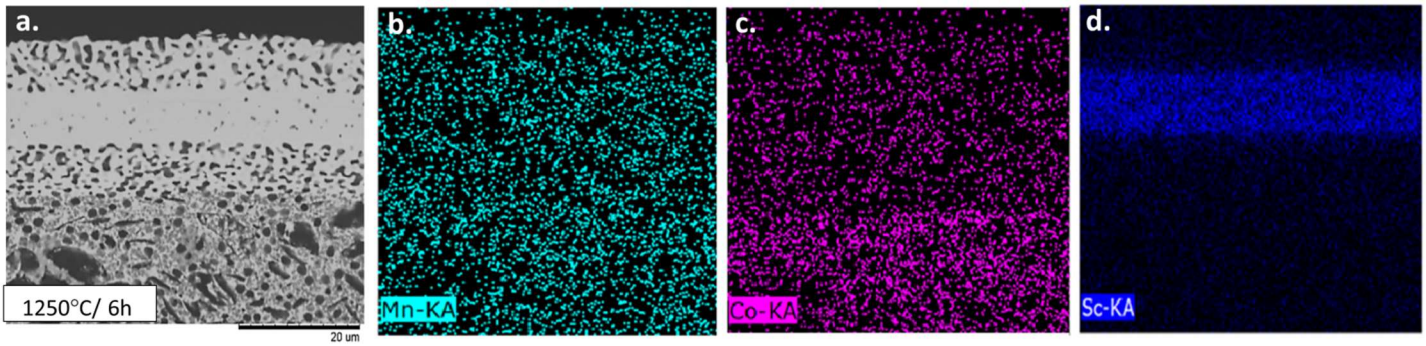

Figure 4:

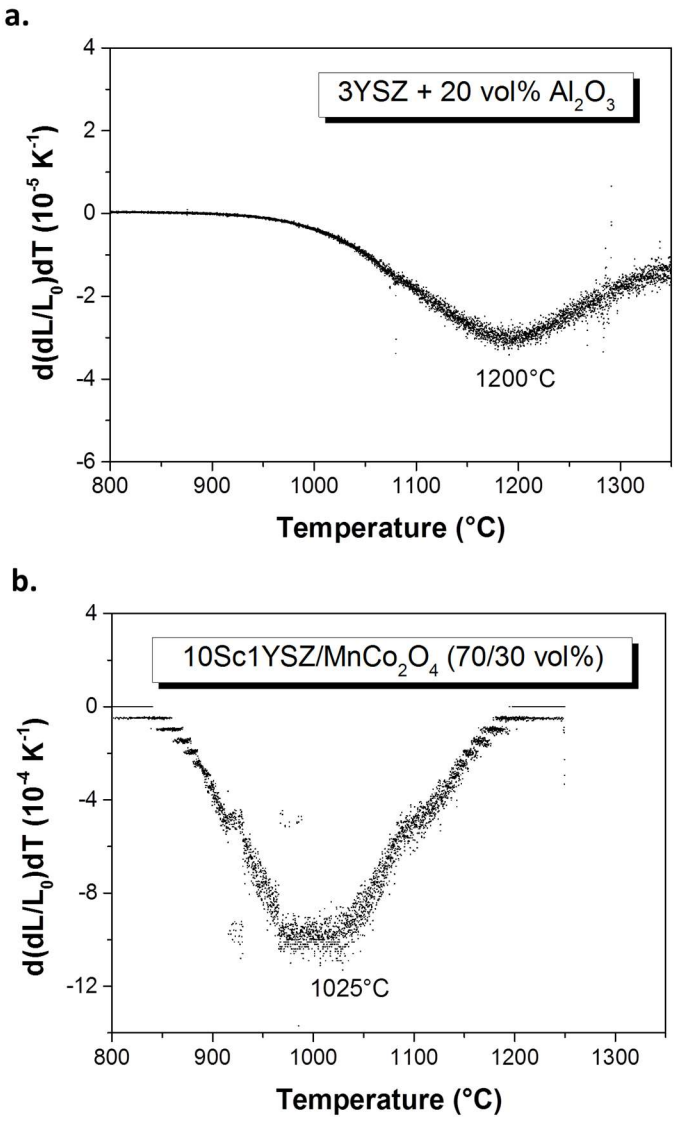
a.
3YSZ + 20 vol% Al2O3
d(dL/L0)dT (10-5 K-1)
1200°C
Temperature (°C)
b.
10Sc1YSZ/MnCo2O4 (70/30 vol%)
d(dL/L0)dT (10-4 K-1)
1025°C
Temperature (°C)

Figure 5:

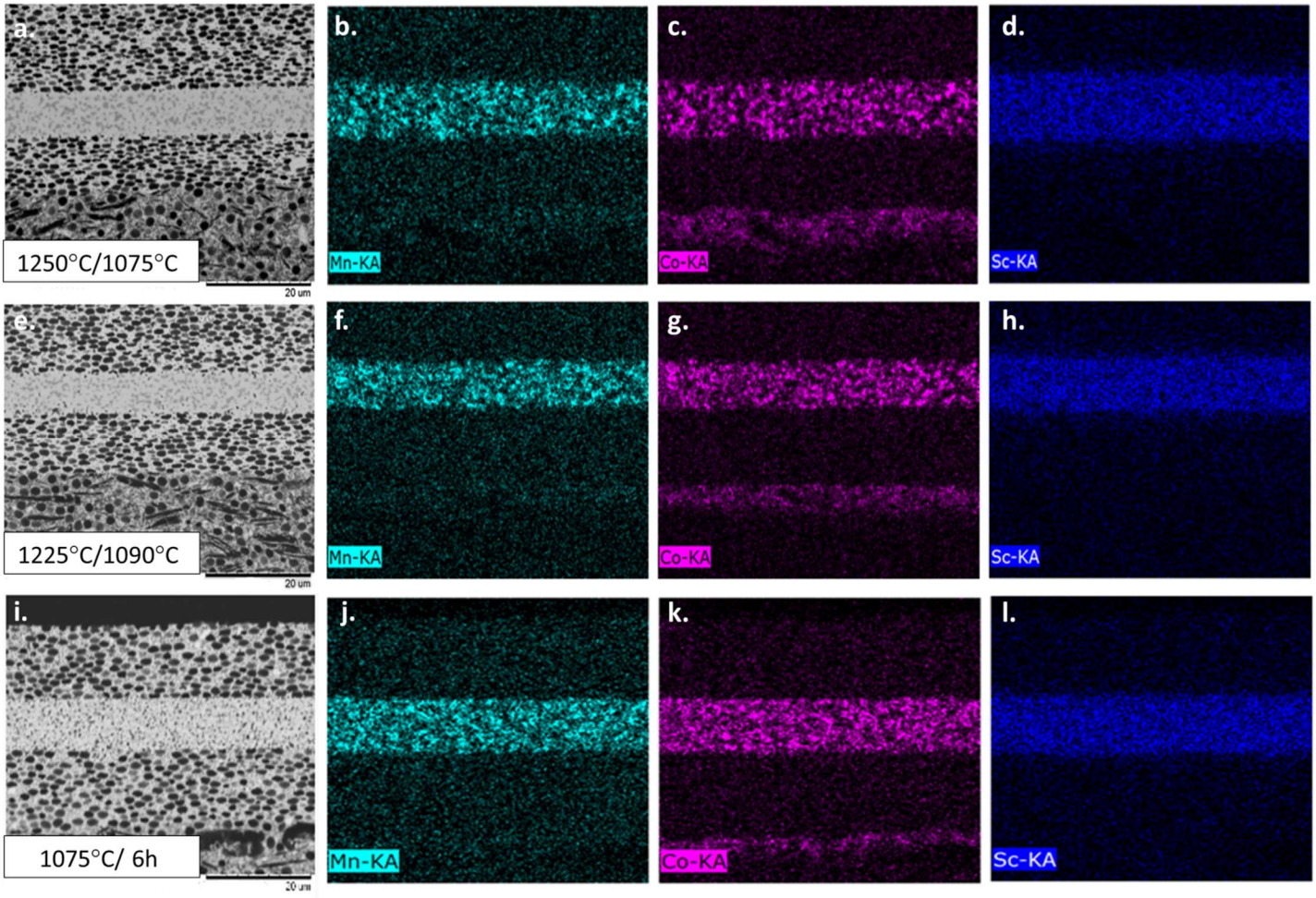
a.
1250°C/1075°C
20 um
b.
Mn-KA
c.
Co-KA
d.
Sc-KA
e.
1225°C/1090°C
20 um
f.
Mn-KA
g.
Co-KA
h.
Sc-KA
i.
1075°C/ 6h
20 um
j.
Mn-KA
k.
Co-KA
l.
Sc-KA

Figure 6:

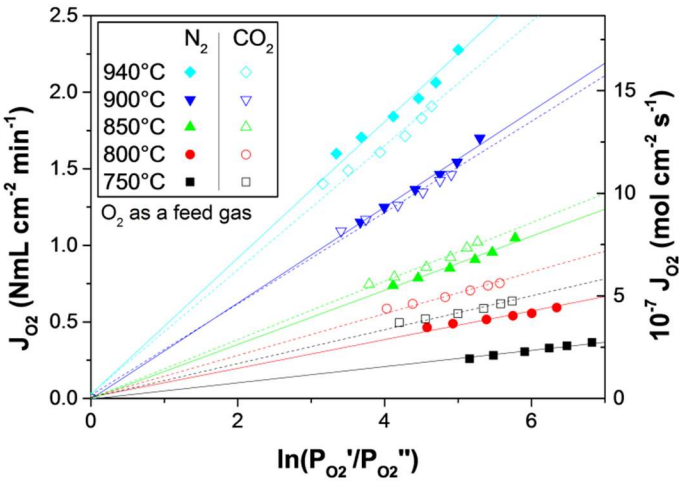
N2
CO2
940°C
900°C
850°C
800°C
750°C
O2 as a feed gas
JO2 (NmL cm-2 min-1)
10-7 JO2 (mol cm-2 s-1)
ln(PO2'/PO2")
0.0
0.5
1.0
1.5
2.0
2.5
0
5
10
15
0
2
4
6

Figure 7:

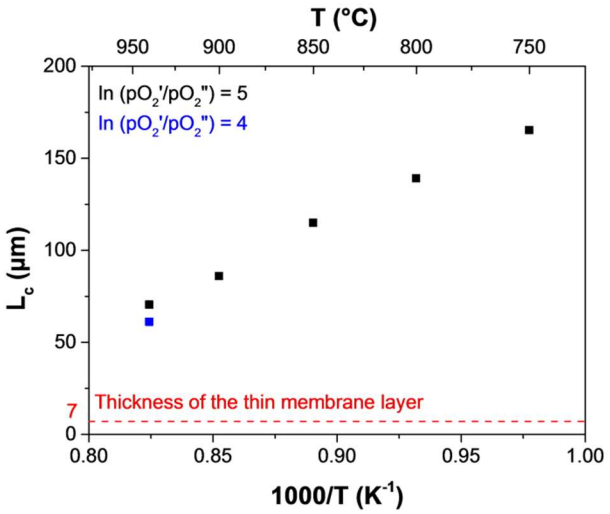
T (°C)
950
900
850
800
750
200
150
100
50
7
0
L_c (µm)
ln (pO_2'/pO_2") = 5
ln (pO_2'/pO_2") = 4
Thickness of the thin membrane layer
0.80
0.85
0.90
0.95
1.00
1000/T (K^{-1})

Figure 8:

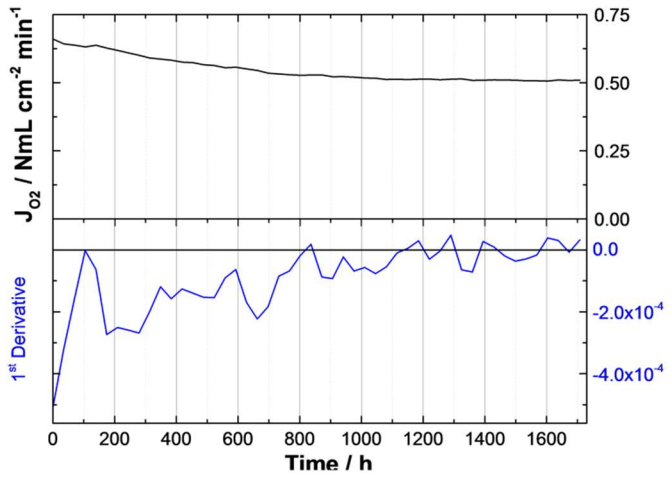
J_{O2} / NmL cm^{-2} min^{-1}
0.75
0.50
0.25
0.00
0.0
-2.0x10^{-4}
-4.0x10^{-4}
1st Derivative
0
200
400
600
800
1000
1200
1400
1600
Time / h

Figure 9:

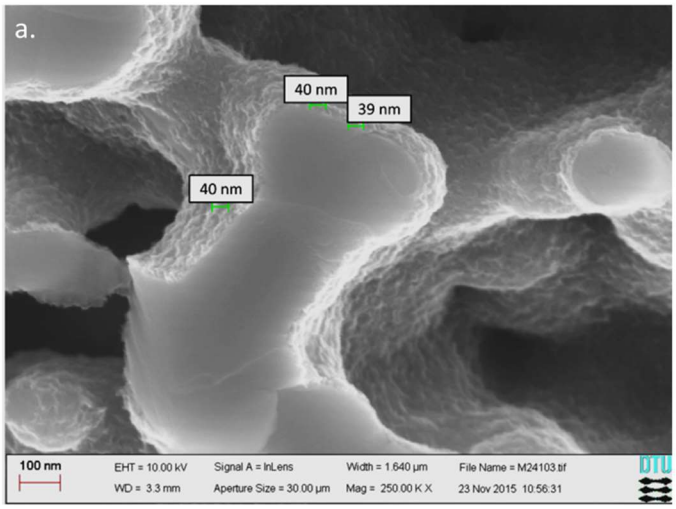
a.
40 nm
39 nm
40 nm
100 nm
EHT = 10.00 kV
WD = 3.3 mm
Signal A = InLens
Aperture Size = 30.00 µm
Width = 1.640 µm
Mag = 250.00 K X
File Name = M24103.tif
23 Nov 2015 10:56:31
DTU

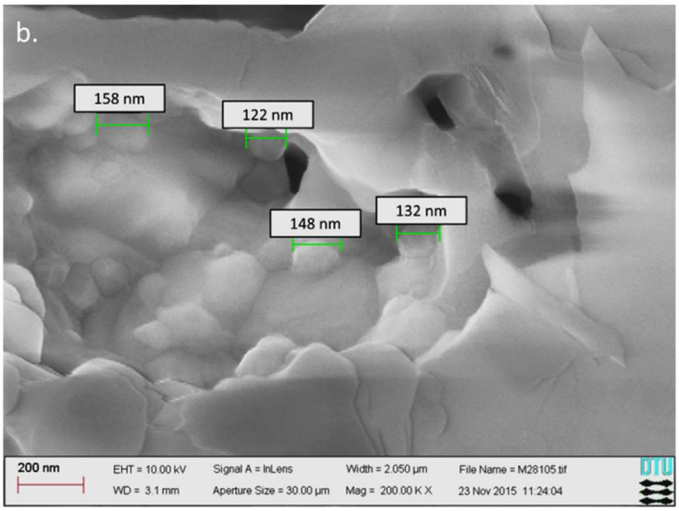
b.
158 nm
122 nm
148 nm
132 nm
200 nm
EHT = 10.00 kV
WD = 3.1 mm
Signal A = InLens
Aperture Size = 30.00 µm
Width = 2.050 µm
Mag = 200.00 K X
File Name = M28105.tif
23 Nov 2015 11:24:04
DTU

Table 1:

Name (Code)	Heating rate step 1 (°C/min)	Holding step 1	Heating rate step 2 (°C/min)	Holding step 2	Heating rate step 3 (°C/min)	Holding step 3	Cooling rate step 1 (°C/min)	Holding step 4	Cooling rate step 2 (°C/min)
Conventional sintering at 1250°C **(CS1250)**	0.25	600°C / 4h	1	1250°C / 6h	-	-	1.67	-	-
Conventional sintering at 1075°C **(CS1075)**	0.25	600°C / 4h	1	1075°C / 6h	-	-	1.67	-	-
Two-step sintering at 1250°C/1075°C **(TSS1250/1075)**	0.25	600°C / 4h	1	1075°C / 1min	25	1250°C / 3min	25	1075°C / 6h	1.67
Two-step sintering at 1250°C/1075°C **(TSS1225/1090)**	0.25	600°C / 4h	1	1090°C / 1min	25	1225°C / 3min	25	1090°C / 6h	1.67

Table 2:

Temperature (°C)	Atmosphere			
	Air/N_2	Air/CO_2	O_2/N_2	O_2/CO_2
	Oxygen permeation fluxes (Nml $cm^{-2}min^{-1}$) / $ln(pO_2'/pO_2'')$			
750	0.29 / 5.496	0.39 / 4.660	0.37 / 6.824	0.64 / 5.737
800	0.49 / 4.975	0.43 / 4.571	0.59 / 6.344	0.75 / 5.569
850	0.83 / 4.447	0.52 / 4.384	1.05 / 5.778	1.02 / 5.266
900	1.26 / 4.036	0.66 / 4.136	1.70 / 5.296	1.46 / 4.907
940	1.41 / 3.920	0.81 / 3.978	2.28 / 5.004	1.91 / 4.642